OMICS A Journal of Integrative Biology
Volume 18, Number 8, 2014

DOI: 10.1089/omi.2013.0175

Lipidomics for Clinical Diagnosis: Dye-Assisted Laser Desorption/Ionization (DALDI) Method for Lipids Detection in MALDI Mass Spectrometry Imaging

Karim Arafah,[1*] Rémi Longuespée,[1*] Annie Desmons,[1] Olivier Kerdraon,[1,2] Isabelle Fournier,[1] and Michel Salzet[1]

Abstract

Lipid-based biomarkers for research and diagnosis are rapidly emerging to unpack the basis of person-to-person and population variations in disease susceptibility, drug and nutritional responses, to name but a few. Hence, with the advent of MALDI Mass Spectrometry Imaging, lipids have begun to be investigated intensively. However, lipids are highly mobile during tissue preparation, and are soluble in the solvent used for matrix preparation or in the fixing fluid such as formalin, resulting in substantial delocalization. In the present article, we investigated as another alternative, the possibility of using specific dyes that can absorb UV wavelengths, in order to desorb the lipids specifically from tissue sections, and are known to immobilize them in tissues. Indeed, after lipid insolubilization with chromate solution or chemical fixation with osmium tetroxide, heterocyclic-based dyes can be directly used without matrix. Taking into account the fact that some dyes have this matrix-free capability, we identified particular dyes dedicated to histological staining of lipids that could be used with MALDI mass spectrometry imaging. We stained tissue sections with either Sudan Black B, Nile Blue A, or Oil Red O. An important advantage of this assay relies on its compatibility with usual practices of histopathological investigation of lipids. As a new method, DALDI stands for Dye-Assisted Laser Desorption Ionization and allows for future clinical and histopathological applications using routine histological protocols. Additionally, this novel methodology was validated in human ovarian cancer biopsies to demonstrate its use as a suitable procedure, for histological diagnosis in lipidomics field.

Introduction

Lipid disorders can arise from defects in lipid metabolism and are characterized by the accumulation of various types of lipids (e.g., cerebrosides, gangliosides, or sphingomyelin) in different organs. The dysfunction of specific enzymes that normally metabolize the lipids in the cell results in their accumulation at cellular level, in tissues and organs as well. Lipid metabolism defects are responsible, for example, for Gaucher disease, coronary diseases, and Fabry disease.

In light of these lipid-related diseases, Fujiwaki et al. (2002; 2004; 2008) have demonstrated that the ratios of ceramide/monohesoxylceramide, ceramide/sphingomyelin, and glucosylceramide/sphingomyelin are significantly different between Gaucher disease and Fabry disease. Similarly, Takeromi et al. (1996) have illustrated the utility of Matrix Assisted Laser Desorption/Ionization (MALDI) as a method for glycosphingolipid analysis in the human brain. All of these studies were performed using the same technique of extraction, centrifugation, and sodium carbonate treatment, following lipid separation (Bligh and Dyer, 1959; Lebaron and Folch, 1959), occasionally with saponification treatment for sulfatide quantification (Calvert et al., 1981). In the early 90's, MALDI profiling and imaging have raised for the direct analysis of biological tissue by mass spectrometry (Caprioli et al., 1997; Fournier et al., 2003; Jimenez et al., 1998). In parallel to the numerous developments performed for proteins/peptides analyses (Bonnel et al., 2011; Calligaris et al., 2013; Caprioli, 2005; El Ayed et al., 2010; Franck et al., 2009a, 2010; Longuespee et al., 2012a, 2013a, 2013b, van Remoortere et al., 2010), lipids are now being intensively

[1]Laboratoire de Protéomique, Réponse Inflammatoire, Spectrométrie de Masse (PRISM), Université de Lille 1, Cité Scientifique, Villeneuve D'Ascq, France
[2]Laboratoire d'Anatomie et de Cytologie Pathologiques, CHRU Lille, Lille Cedex, France.
*Co-authors.

investigated using this method. Ishida et al. and Rujoi et al. have both used this technology for the localization of phospholipids and/or sphingomyelins in zooplankton, bacteria (Ishida et al., 2002; 2003, 2005) or in calf eyes (Rujoi et al., 2003, 2004; Yappert et al., 2003). Along the same lines, imaging of phospholipids and cholesterol after direct analysis was first done using TOF-SIMS in mice, which allowed for the mapping of these molecules in a tissue section (Touboul et al., 2004), then in MALDI (Benabdellah et al., 2010). MALDI-MSI was also used to generate LIPID MAPS of brain and liver tissue from primates, mice and rats, or invertebrate (Astigarraga et al., 2008; Burnum et al., 2009; Colsch and Woods, 2010; Franck et al., 2009a; Garrett and Dawson, 2009; Hayasaka et al., 2009; Landgraf et al., 2009; Meriaux et al., 2010, 2011; Mikawa et al., 2009; Murphy et al., 2009; Snel and Fuller, 2010; Sparvero et al., 2012; Sugiura et al., 2008, 2009; Vidova et al., 2010; Wang et al., 2012, 2014).

However, important precautions before lipids analysis have to be taken during the sample preparation for matrix choice and application. Although issues concerning ion suppression and correlation of lipids localization in brain using MALDI-MSI and other lipids analysis methods were previously described (Veloso et al., 2011), little has been investigated concerning lipid delocalization during sample preparation for MALDI analysis. Lipids are highly mobile during tissue preparation and are soluble in the solvent that is used for matrix preparation, resulting in their substantial delocalization. For example, usual aldehydic fixatives wash out most of the phosphatidylserine (Maneta-Peyret et al., 1999) and alcohol (ethanol) dehydration during paraffin processing removes most of the polar lipids.

The two classical histological methods using formalin or glutaraldehyde have been widely described to fix the biological specimen through protein crosslinking but do not target lipids. In order to keep lipids and avoid their subsequent delocalization on tissue using such standard procedures, we describe a novel protocol that preserves lipids on tissue slices using osmium tetroxide or post-chromization followed by Baker's fixation. While formalin is a fixative used worldwide to preserve histological features, not all of the lipid classes can be fixed on tissue, and turned insoluble after processing the tissue slices with organic solvents for MALDI imaging purposes. It has been shown that formalin fixation helps to protect some phospholipids from delocalization after deposition of the MALDI matrix solution prior imaging (Carter et al., 2011). Nevertheless, as a protein crosslinker, formalin cannot avoid lipid diffusion or removal after extensive contact with lipophilic solvents. Baker's fixative, designed for the preservation of phospholipids, uses formalin together with calcium and cadmium chlorides (the last, being expensive, has subsequently been replaced by cobalt nitrate). While phospholipids (phosphatidylcholine (PC) and sphingomyelin (SM)) are preserved as demonstrated in MALDI imaging of rat brain by Carter et al. (2011), they are not prevented from diffusing into the fixing fluid and are still removable by solvents that solubilize lipids (Clark, 1947).

To avoid this outcome, sublimation was used for solvent-free deposition of 2,5-dihydroxybenzoic acid for on-tissue lipidomics studies by MALDI-MSI (Murphy and colleagues (2009). In parallel, Nanostructure Assisted Laser Desorption Ionization (NALDI) can also be considered as a matrix-free alternative to perform MALDI-MSI of lipids (Guenin et al., 2009).

In the present study, we investigated another approach to analyze lipids directly on tissue by MALDI imaging. This approach takes into account the sample preparations followed by the hospital pathologists and the possibility of using specific dyes that can absorb UV wavelengths in order to desorb the lipids specifically from tissue sections. Some lipophilic dyes share a common molecular structure with heterocyclic-based dyes (e.g., heterocyclic-based dyes, cores absorbing UV photons and have proven to desorb lipids). For instance, Oil Red O dye in propylene glycol has been historically used to immobilize lipids from fresh or fixed frozen tissue (Clark, 1947) and to stain structural lipids in cells and tissues. After lipid fixation with chrome (Kotelnikov and Litinskaya, 1981; Purbach et al., 2002) or with osmium tetroxide (Collin et al., 1973, 1974; Litman and Barrnett, 1972; Riemersma, 1968), heterocyclic-based dyes can be directly used without a matrix. Our team presented for the first time the use of particular dyes that had matrix-free capabilities for MALDI imaging of lipids in rat brain sections and in pathological context as well. Recently, Francese et al. (2013) have also shown that curcumin, which is a phenolic compound, can be used as a MALDI matrix for imaging lipids in skin and lung tissue.

Combining on-tissue lipid preservation and staining, we mapped lipids using the lipophilic dyes Sudan Black B, Nile Blue A, or Oil Red O by MALDI imaging without any additional matrix coating onto the tissue. Moreover, to perform histomolecular images of lipids with DALDI strategy, no use of automatic micro/nano-spotting or spraying devices was required. This new method, that we called DALDI, will allow for clinical investigations using a protocol that is identical to typical histopathological techniques, without requiring any additional tissue treatment.

Materials and Methods

Reagents

Ethanol (EtOH), Chromasolv Plus water for HPLC (H_2O), Nile Blue A, Oil Red O, and Sudan Black B were all certified by the Biological Stain Commission and purchased from Sigma-Aldrich (Saint Quentin Fallavier, France). The aqueous solution of 4% osmium tetroxide (OsO_4^-) was purchased from Electron Microscopy Sciences (Hatfield, England). The filters (330 mm in diameter) were purchased from Fisher (Elancourt, France).

Preparation of staining solutions

Nile Blue A was diluted in water (30 mg/mL), while the Oil Red O and Sudan Black B were diluted in a 60% ethanol solution (30 mg/mL). After stirring, all staining solutions were filtered.

Sample preparation

Rat brain cryosections. Frozen rat brains were cut into 10 μm-thick tissue sections using a cryostat Leica CM1510S (Leica Microsystems, Nanterre, France). The sections were applied onto ITO-coated conductive glass slides (Bruker Daltonics, Bremen, Germany) and dried in a desiccator for 10 min.

Lipid fixation. The tissue sections were fixed in the tetroxide osmium solution prior to staining with Sudan Black B for 15 min. The rat brain slices stained with Nile Blue A were

previously fixed in Baker's fixative solution overnight and post-chromized for 2 h prior to lipid staining.

Fixation of rat brain lipids with osmium tetroxide. A 1% osmium tetroxide solution was prepared in water from the 4% stock solution. The 1% working solution (50 μL) was deposited onto the rat brain slice and left for lipid fixation for 20 min in the dark.

Baker's fixation of lipids in tissue sections. Baker's solution was prepared by mixing 10 mL of a 10% $CaCl_2$ solution with 10 mL of concentrated formalin in 90 mL of HPLC-grade water. Slices were incubated overnight in Baker's solution for global tissue fixation and then washed in HPLC-grade water (three times for 5 min each). Slices were then incubated in 50 mL of a 5% $K_2Cr_2O_7$ solution (m/v) and 7.5 mL of 4% formalin, all diluted in distilled water (HPLC grade). After three washes in HPLC-grade water for 5 min each, the slices were dried for 15 min.

Tissue imaging

Fluorescence microscopy imaging of lipids. After staining with Nile Blue A, entire rat brain coronal section was imaged at 10X optical magnification using the wide-field microscope Leica AF 6000 LX and DAPI as UV filter.

Mass Spectrometry Imaging of lipids and molecular assignments. Molecular images were acquired using an UltraFlex II MALDI-TOF/TOF instrument (Bruker Daltonics, Bremen, Germany) equipped with a Smartbeam laser with a repetition rate up to 200 Hz that was controlled by FlexControl 3.0 (Build 158) software (Bruker Daltonics). Images were obtained in the positive and negative reflector mode, and MALDI MS spectra were acquired in the 200–1500 m/z range. A total of 500 spectra were acquired at each spot at a laser frequency of 100 Hz and a spatial resolution set to 200 μm. The images were saved and reconstructed using FlexImaging 2.1 (Build 15) (Bruker Daltonics). The molecular assignments were performed using databases from LipidMaps (Lipid MS Predict application) in order to predict lipid species according molecular ions (m/z) and with a maximum difference between experimental and theoretical m/z values set to 0.3 μ. The on-tissue lipid fragmentation was carried out using the lift-negative method from Bruker, and matching of the daughter ions was performed using the glycerophospholipid databases in negative mode from LipidMaps.

Statistical data analysis

Symbolic discriminant analysis (SDA) was used to analyze the lipid profiles. SDA determines discriminatory signals and builds functions using these signals that distinguish sample populations based on their classification. Peak lists from MALDI spectra obtained using Flex Analysis 2.4 and Flex Control 2.5 that were input into the analysis program were clustered according to similarity, using a presence/absence criterion. Statistical analyses were carried out using the ClinProTools 2.2 Software. For the statistical analyses, the mass spectra were internally recalibrated on common peaks (also known as spectral alignment) and normalized to the total ion count. An average spectrum created from all single spectra was used for a peak selection and to define integration ranges. These integration ranges were used to obtain the intensities or areas of the single spectra. The signal intensities were used for all calculations. For the principal component analysis (PCA) and the hierarchical clustering, the individual peak intensities were standardized across the data set (Franck et al., 2009b). The PCA was carried out using Pareto scaling, which uses the square root of the standard deviation as a scaling factor to reduce the dominance of large-scale intensity changes in the matrix and other high-abundance ions, as these may mask variation in lower abundance ions during the PCA. The overall outcome of the PCA is greatly affected by the fact that ions related to the matrix coating and other endogenous molecules can mask the underlying relevant information. A plot of principal component 1 (PC1) versus principal component 2 (PC2) was chosen since these components resulted in the highest overall degree of separation of the spectra within the PCA scores plots. Under the unsupervised PCA, each spectrum is classed as an individual, so the principal components that are selected account for the greatest separation of each individual spectrum. M/z ion peaks responsible for the greatest variations are then plotted in the loading plots.

Ovarian cancer cryosections and fixation

Ovarian cancer biopsies were obtained with informed consent and institutional review board approval (CCPPRBM Lille: CP 05/83), from patients undergoing any ovarian tumor resection at Hospital Jeanne de Flandre. Patient information was collected, including gender, age, treatment received before and after surgery, extent of surgery, current status (alive, alive with progressive disease, deceased, and cause of death) and survival from the time of original pathologic diagnosis. Samples were collected at the time of surgery, immediately frozen and stored at $-80°C$ until analysis.

Sections (12 μm thick) were prepared from fresh ovarian cancer tissue using a cryostat Leica CM1510S (Leica Microsystems, Nanterre, France) and applied onto ITO-coated conductive glass slides (Bruker Daltonics). The slices were first fixed in Baker's fixative solution overnight and then post-chromized for 2 h for nonsolubilized heterophasic lipids (see protocol above). After drying in a desiccator for 15 min, the slices were incubated in the Nile Blue A or the Oil Red O staining solution for 30 min or 15 min, respectively. Histopathologic diagnoses were made from subsequent H&E-stained sections by a pathologist blinded to the original clinical diagnosis.

Results

Lipid fixation and Dye-Assisted Laser Desorption/Ionization (DALDI) MSI of lipids

As mentioned in the introduction, the major problems with lipids are their plasticity, high diffusion, and high solubility (Maneta-Peyret et al., 1999). These factors make it difficult to ensure that the lipids do not diffuse during tissue preparation and make matrix application difficult. To solve these problems, we studied lipid-specific tissue fixation before undertaking any other tissue treatment. For this purpose, we have used either osmium tetroxide or chrome fixation based on electron microscopy protocols (Collin et al., 1973, 1974; Kotelnikov and Litinskaya, 1981; Litman and Barrnett, 1972;

Purbach et al., 2002; Riemersma, 1968). The fixation of the lipids should prevent their delocalization within the tissue sections during manipulations prior to MS analysis. Because quality of the matrix coating is one of the difficulties in lipid imaging and because lipids are rather volatile compounds that easily desorbed under laser irradiation, we aimed to use staining molecules as a MALDI matrix. In theory, it should be possible to fix lipids using Baker's solution, stain the tissue sections for histological analysis (Lillie, 1943), and then reuse the same sections for MALDI-MSI without any further treatment of the tissue. We called this technique Dye-Assisted Laser Desorption Ionization (DALDI).

Fixed tissue section was incubated in Nile Blue A dye and the distribution of lipids was revealed in coronal slice of rat brain using UV microscopy (Fig. 1, see picture). The histological mechanism of the staining of lipids is invariably a function of the physical properties of the dye being more soluble in the lipid to be demonstrated than in the vehicle solvent. The polyazo group of dyes include the oil red series, the Sudan red series, and the Sudan blacks. Thus, we assessed the utility of acidic and slightly basic diazo dyes, namely Oil Red O (Fig. 1A) and Sudan Black B (Fig. 1B), respectively, and the phenoxazone basic dye Nile Blue A (Fig. 1C) for imaging lipid species using MALDI technology.

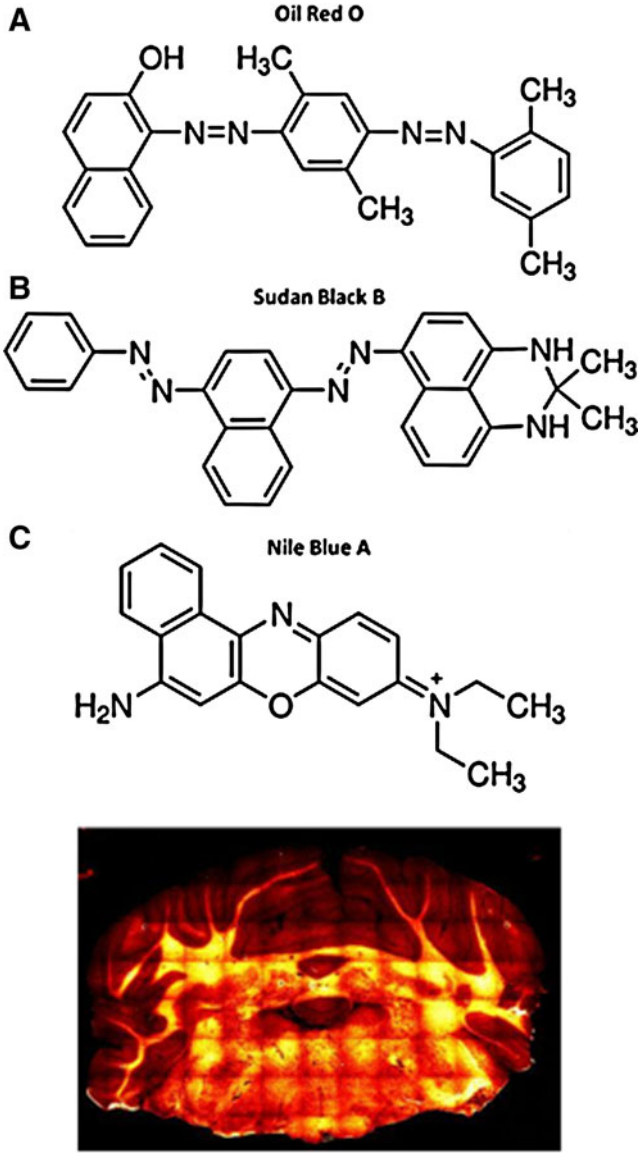

FIG. 1. Chemical formula of the tested dyes **(A)** Oil Red O, **(B)** Sudan Black B, and **(C)** Nile Blue A. Inset picture represents a wide-field fluorescence imaging microscopy of rat brain tissue section after Nile Blue A staining.

In anatomopathology, Oil Red O is used to stain cholesteryl esters and neutral fats such as triacylglycerols, and Sudan Black B stains triglycerides and lipoproteins. Nile Blue A reveals neutral and acidic lipids (e.g., phospholipids such as phosphatidylcholine). Nile Blue A, Oil Red O, and Sudan Black B absorb UV wavelengths (340 nm, 359 nm, and 415 nm, respectively) that are included within the MALDI absorption wavelength range of the AutoFlex smartbeam UV laser. Rat brain sections were fixed with Baker's fixation solution, post-chromized, and then stained with the dyes. For sections stained with Sudan Black, an additional step relying on a fixation with osmium tetroxide was added before coloration in order to ensure that no delocalization could occur due to the presence of ethanol as a vehicle for the dissolution of the dye.

A comparison of the mass spectra and molecular images between section directly imaged after staining with Sudan Black B (Fig. 2A and B) and section fixed with osmium tetroxide prior imaging using the same dye (Fig. 2C and D) demonstrated that fixed tissue yields better lipid detection and structure preservation. A comparison of the molecular images for identical ions in both cases showed a very good localization with respect to the brain anatomy after fixation with osmium tetroxide (Fig. 2D). Triglycerides, sulfatides, diglycerides, sphingomyelin, phospholipids, and fatty acids were more easily detected using Sudan Black B with fixation (Table 1). Importantly, the spatial distribution of the lipids detected using Sudan Black B without fixation (Table 1) was completely lost (Fig. 2C) following incubation in the staining solution, most likely a result of the ethanol/water vehicle.

In the case of Nile Blue A, following fixation in Baker's solution and post-chromization of the lipids for their insolubilization, mass spectra of lipid ions and their subsequent histological distribution were recorded (Fig. 3) both in reflectron negative (Fig. 3A and C) and reflectron positive (Fig. 3B and D) modes. In both modes of analysis, diglycerides, sphingomyelin, phospholipids, triglycerides, and sulfatides were localized with respect to the rat brain anatomy (Fig. 3C, Table 2). These data reflect complementary methods for lipid localization due to the possibility of accessing both negative and positive modes and the molecular images reinforce this assumption. These experiments also demonstrate that well-established lipid dyes in histology can advantageously replace classic MALDI matrices in lipidomics through DALDI-MSI. Therefore, it is possible to prepare a tissue section for histopathological studies of lipids and use the same section for DALDI-MSI.

Application to pathology: Ovarian cancer

In order to investigate these developments in a pathologic context, we tested Nile Blue A and Oil Red O to stain tissue sections of serous ovarian carcinoma following osmium

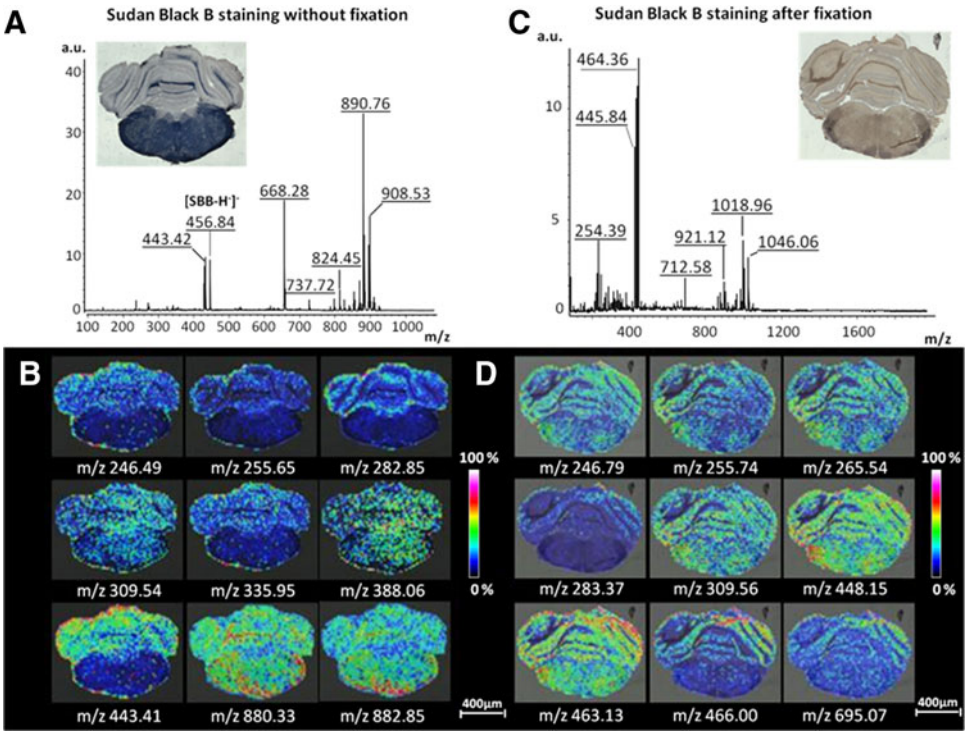

FIG. 2. A comparison of tissue profiling and imaging of tissue sections of rat brain following osmium tetroxide fixation and staining with Sudan Black B. **(A, B)** MALDI mass spectra recorded from the tissue in reflectron negative mode following Sudan Black B staining without **(A)** or with **(B)** osmium tetroxide fixation. **(C, D)** Molecular images reconstructed for various ions after tissue imaging in the negative mode following Sudan Black B staining without **(C)** or with **(D)** osmium tetroxide fixation.

fixation before DALDI-MSI analysis in negative reflectron mode (Fig. 4A and B, Table 3). Principal component analyses were performed from the DALDI images datasets, allowing for the detection of two defined ions clusters (Fig. 5).

As observed in Table 3, lipid species were detected using Nile Blue A and Oil Red O as well. However, in the PCA analyses, some specific ions were detected in the tumor region using each dye. Using Nile Blue A, interesting ions were detected in the tumor region following the PCA analyses. Lipid annotations with Lipid Mass Predict theoretical databases included palmitic acid C16:0 (255.63), arachidonic acid C20:4 (303.29), and stearic acid C18:0 (283.63) (Table 3). Using Oil Red O, different ions as compared to Nile Blue A were depicted in the tumor after PCA analysis. These ions may correspond to docosahexaenoic acid C22:6 (407.35), phosphatidic acid PA C17:1 (421.23), and sphinganine CerP2:0 (422.23), according to Lipid Mass Predict.

These data are in line with previous studies that have shown that the fatty acid composition of ceramide and sphingomyelin isolated from tissues are significantly different: the predominant acids are oleic (18:1) in ceramide and palmitic (16:0) in sphingomyelin, which contains many more other forms of saturated acids (Rylova et al., 1998). These differences are characteristic of both normal and tumor tissues. Sphingoid base compositions of ceramide and sphingomyelin in normal tissue are identical: the major component is sphingenin (over 96%), while ceramides from tumors contain, in addition to sphingenin, a significant amount of

Table 1. Comparison of Lipid Species Detected after Application of Black Sudan B With or Without Previous Lipid Fixation with Osmium Tetroxide

Brain section DALDI-MSI with Sudan Black B in negative mode (without osmium tetroxide fixative)					
Experimental mass	*Theoretical mass*	*Δ (u.m.a.)*	*Identification [M-H]⁻ species*	*Other possibilities*	*Intensity*
249.20	249.19	0.01	C16:3		509.80
880.33	880.51	0.18	PS(22/5:22/6)		357.85
882.85	882.73	0.12	PC(O-18:0/26:2) or PC(O-18:1/26:1)		402.36
890.76	890.63	0.13	ST 42:1		4224.96
904.55	904.62	0.07	ST-OH 42:2	PS 45:6 904.60	109.09
906.72	906.62	0.1	ST-OH 42:1	PS 45:5 906.62	1556.30
1130.14	1130.01	0.13	GL 72:6		33.58

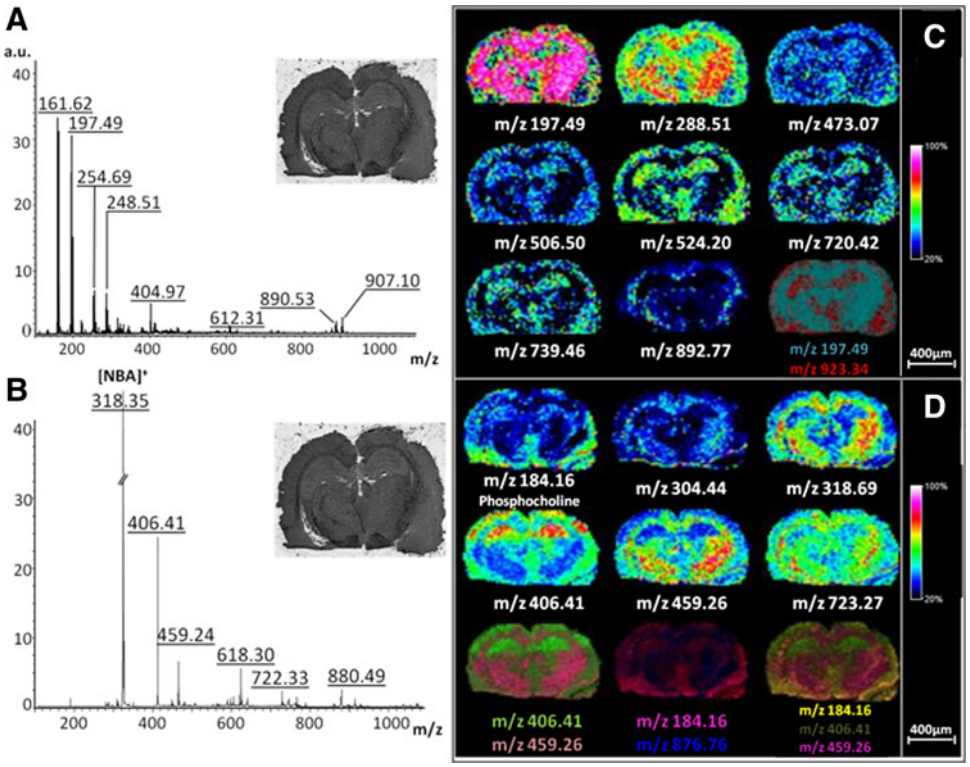

FIG. 3. A comparison of tissue profiling and imaging from tissue sections of rat brain following chrome fixation and Nile Blue A staining. **(A, B)** A comparison of the MALDI mass spectra recorded from the tissue in the negative **(A)** and positive **(B)** reflectron mode. **(C, D)** Molecular images reconstructed for various ions following Nile Blue A staining after chrome fixation in the negative mode **(C)** and positive reflectron mode **(D)**.

sphinganine. In the sphingomyelins isolated from tumors, sphinganine content is significantly lower than in ceramides and depends on the type of tumor (Dyatlovitskaya et al., 1997; Rylova et al., 1998). Moreover, in order to investigate the structural characterization of the lipids detected on the ovarian biopsy section using Nile Blue A, tandem mass spectrometry was successfully performed on several ions including the m/z 886.13 (Fig. 6). This ion was detected with a higher intensity in the cancerous region of the ovarian tissue section. After isolation and fragmentation, the daughter ions were recorded and the identity of the lipid elucidated according the lipid family core. The structural elucidation of the m/z 886.13 has revealed the characteristic ions from the glycerophosphatidylinositol (PI) lipid, namely phosphate, inositol phosphate ions, and the glycerol core esterified with the stearic acid (C18:0) and the arachidonic acid (C20:4). As a result, the entire MS/MS spectrum of this PI (C18:0/C20:4) was compared to theoretical MS/MS datasets from LIPID MAPS bank (Table 4). Amongst the 20 theoretical daughter ions, 17 were found in the DALDI-MS/MS experiment of the PI (C18:0/C20:4). The three undetected ions corresponded to the loss from the precursor ion of sn2 acyl chain with or without the inositol, and the inositol phosphate with a double dehydration.

Considering our data, the use of Nile Blue A and Oil Red O as coloring agents to study ovarian carcinoma not only

TABLE 2. COMPARISON OF LIPID SPECIES DETECTED IN POSITIVE OR NEGATIVE MODE AFTER APPLICATION OF NILE BLUE A

Brain section DALDI-MSI Nile Blue A in negative mode

Experimental mass	*Theoretical mass*	*Δ (u.m.a.)*	*Identification [M-H]⁻ species*	*Other possibilities*	*Intensity*
506.31	506.36	0.05	PC(O-18:1/0:0)		41.16
524.2	524.27	0.07	PE 22:6	PE(18:0) 524.29	44.53
720.42	720.46	0.04	PE 35:6	PC(32:6) 740.46	48.13
739.46	739.58	0.12	GL 44:5	GL(45:5) 739.62	55.23
782.59	782.65	0.06	CerP(d18:1/24:0)		38.76
811.58	811.67	0.09	SM 24:1	PA(44:2) 811.62	78.54
882.47	882.52	0.05	PS 44:10		102.15
892.70	892.63	0.07	ST 42:0		124.26
923.34	923.47	0.13	PIP 35:4		121.53
1039.91	1040.00	0.09	GL 66:2		67.22

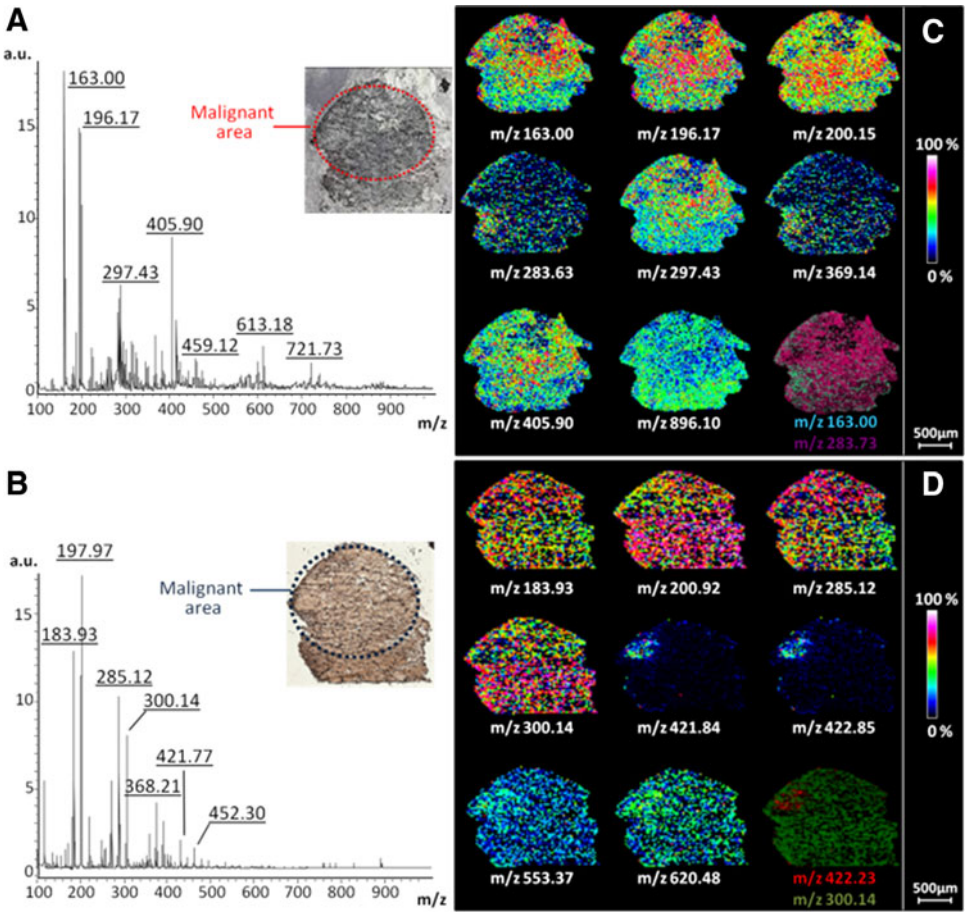

FIG. 4. MALDI mass spectra and molecular images obtained for the analysis of serous ovarian cancer biopsy sections after fixation and staining with different dyes. **(A, B)** A comparison of MALDI mass spectra recorded from the tissue sections in the negative reflectron mode following Nile Blue A **(A)** and Oil Red O **(B)** staining. **(C, D)** Molecular images reconstructed for various ions after tissue imaging in the negative reflectron mode following Nile Blue A **(C)** and Oil Red O **(D)** staining.

TABLE 3. COMPARISON OF LIPID SPECIES DETECTED IN HUMAN OVARIAN CANCER BIOPSIES AFTER APPLICATION OF EITHER OIL RED O OR NILE BLUE A

Ovarian biopsy section DALDI-MSI with Nile Blue A in Negative Mode					
Experimental mass	*Theoretical mass*	*Δ (u.m.a.)*	*Identification [M-H]⁻ species*	*Other possibilities*	*Intensity*
163.00	163.07	0.07	C10:4		7626.05
255.63	255.23	0.4	C16:0		68.22
283.63	283.63	0	C18:0		109.29
285.12	285.15	0.03	C18:6(Ep)	C18:6(Ke)	471.76
291.10	291.19	0.09	C18:4(OH)	C18:3(OH)-cyclo	791.68
297.43	297.25	0.18	C18:1(OH)		345.03
300.45	300.29	0.16	sphinganine Cer0:0		756.37
303.29	303.24	0.05	C20:4		152.44
459.12	459.25	0.13	PA 20:3		200.28
474.10	474.26	0.16	PE 18:3		175.31
579.37	579.49	0.12	TG 33:1		35.15
600.51	600.33	0.18	PS 24:4	SphingosineCer18:0(Cl^-) or Sphinganine Cer18:1(Cl^-) 600.51	109.71
614.50	614.46	0.04	sphingosineHexCer10:0		128.67
721.73	721.70	0.03	TG 44:0	DAG 33:0 721.54	127.61
740.75	740.45	0.3	PC 33:4		449.28
935.26	935.46	0.2	PIP 36:5		34.51
978.46	979.53	0.07	PIP 39:4		31.96

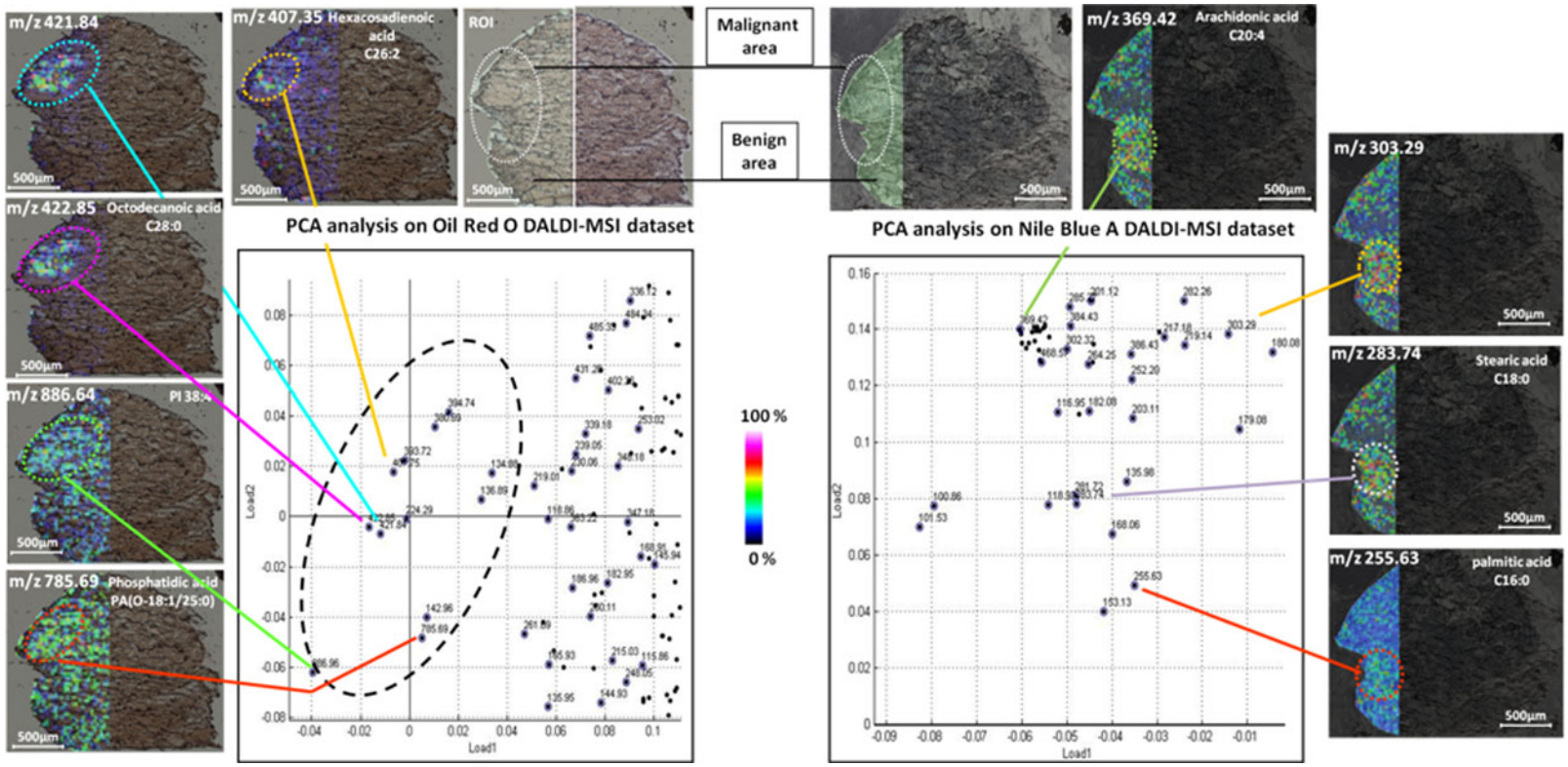

FIG. 5. Reconstructed molecular images of the ions differentially expressed in malignant area of the serous ovarian cancer tissue section based on the PCA from fixed tissue stained with Oil Red O and Nile Blue A.

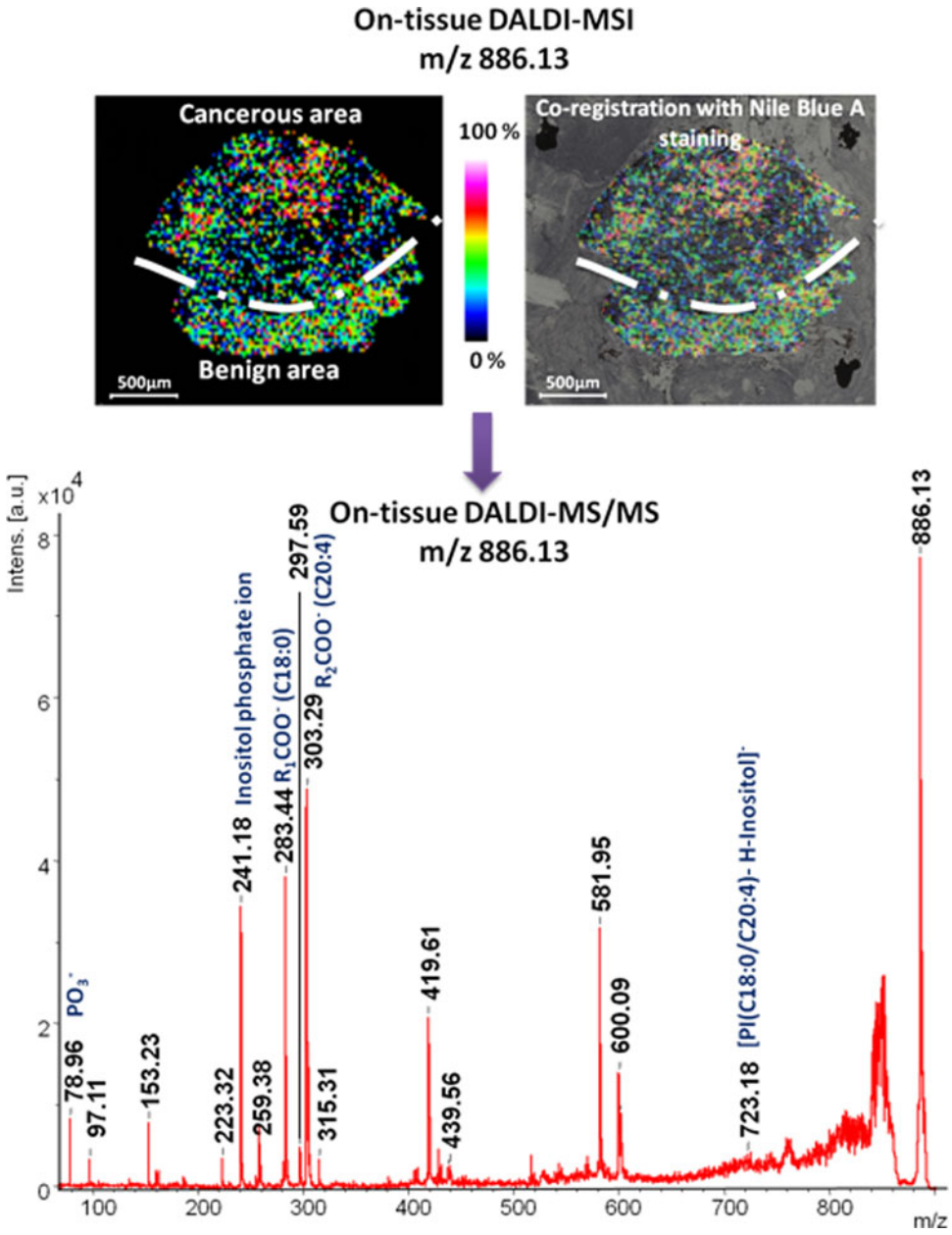

FIG. 6. MS/MS based characterization of the m/z 886.13 ion. Post source decay fragment of m/z 886.13 were recorded and allowed us to identify the originating lipid as a phosphatidyl inositol (C18:0/C20:4). Among the detected fragment peaks, we detected inositol phosphate and the two esterified fatty acids C18:0 and C20:4, respectively, R_1COO^-, R_2COO^- ions.

succeeds in detecting lipids from these tissues by DALDI-MSI, but also revealed the capability of DALDI-MSI to build a translational research in oncology and to highlight potential markers, such as sphingenin and glycerophosphatidylinositol. Interestingly, many studies in the research field of ovarian carcinoma highlighted key roles played by phosphoinositides. For instance, the deregulation of the phosphoinositide-3-kinase pathway is a hallmark in ovarian carcinoma as detected after surgical specimen sampling and diagnosis (Carden et al., 2012). In addition, this enzyme is active in significant fraction of low-grade type I and high grade type II ovarian carcinoma lesions. The first type of lesion implies mutation of the enzyme, whereas the second involves an amplification mechanism (Bast and Mills, 2012).

Discussion

DALDI is a novel technology for mapping lipids in the context of clinical studies. Profiling and molecular images can be easily obtained without any delocalization, especially after osmium or chrome fixation. Furthermore, the technique alleviates difficulties resulting from matrix application by using classic dyes as the MALDI matrix for lipid analysis. This suggests that tissues prepared for histological analyses

Table 4. MS/MS Based Comparison of PI (C18:0/C20:4) Ions Found in Direct Isolation and Fragmentation in Ovarian Tissue Sections and Theoretical Values and Structures (LIPID MAPS)

Ovarian biopsy section DALDI-MSI with Oil Red O in negative mode

Experimental mass	*Theoretical mass*	*Δ (u.m.a.)*	*Identification [M-H]⁻*	*Other possibilities*	*Intensity*
183.93	184	0.07	Pcho		1251.67
200.01	200.1	0.09	C10:1(H_2O)		4630.16
285.12	285.13	0.01	C14:3		2085.36
300.14	300.29	0.15	sphinganine Cer0:0		979.61
305.22	305.24	0.02	eicosatrienoic acid C20:3		102.43
407.35	407.35	0	docosahexaenoic acid C22:6 species	PA (C16:1)	316.87
421.23	421.23	0	phosphatidic acid PA 17:1		1665.04
422.23	422.26	0.03	sphinganine CerP2:0	PE(14:1)	950.02
452.24	452.26	0.02	PE 16:0		332.77
536.38	536.37	0.01	PC 19:0		64.74
552.32	552.33	0.01	PS 20:0	PE 22:0	14
553.37	553.36	0.01	phosphoglyceride PG 21:0	C30:5	73.64
604.40	604.39	0.01	PE 26:1		176.43
620.48	620.46	0.02	PE(O-16:0/12:0)	PE(O-18:0/10:0), PC(25:0/0:0)	40.23
785.66	785.65	0.01	sphingomyelin 22:0	PA(O-18:1/25:0), GL 47:3	35.54
886.64	886.63	0.01	PC 44:7		14.83

of lipids can be directly used to retrieve molecular information without any further treatment of the samples. This method could be implemented in the hospital setting by pathologists since no sprayer or spotter is necessary. Achieving accurate diagnoses in extemporary biopsies is difficult. These diagnoses can be conducted with the same histochemical dyes used by the pathologist. The difference occurs at the level of the analysis. While pathologists base the analysis on tissue coloration to reveal accumulation of lipids, DALDI now allows a molecular diagnosis on the same slide by simply performing a MALDI-MSI analysis without any of the classically known post imaging treatments such as matrix recall for histochemical staining. In function to the lipid species that are targeted by the pathologists, the two strategies to foresee for successful DALDI-MSI experiments are lipid fixation with osmium tetroxide or insolubilization thanks to the use of a mordent solution such as potassium bichromate in the Baker's fixative. The investigation with ovarian cancer tissue demonstrates the feasibility of this concept and that fixation and staining with the specific dyes assessed here (i.e., Nile Blue A and Oil Red O) is very selective and allows for the detection of lipid markers in the tumor region. These data will truly give a new means for pathologists to combine lipid-based morphological and molecular investigations on the same slice, aiming to improve diagnosis.

The next step relies on structural characterizations of the desorbed lipids from the tissues. Moreover, the results obtained using these different lipid-related dyes suggest the possibility to preferentially detect some groups of lipids over others, regarding the working solvent as well as the chemical properties of basic (e.g., Nile Blue A) or acidic dyes (e.g., Sudan Black B or Oil Red O). In comparison, the matrices widely used in low m/z lipidome investigations using mass spectrometry are acidic. As seen in this report, Nile Blue A dissolved in water is more lipophilic with neutral and acidic lipids (highlighted by its affinity for phospholipids and sulfatides in the negative mode), whereas many more lipids were detected in the positive mode according to the basic property of this dye (Table 2). In this latter mode of detection, Nile Blue A detected fatty acids, glycerides, as well as sphingo- and phospholipids. The use of this dye takes advantage in its better partition into hydrophobic tails of lipids instead of water when the slices are incubated in this staining solution. As a consequence of the water vehicle, the weak delocalization can be easily corrected simply by fixing the section in Baker's fixative followed by a post-chromization step.

We first proved the application of DALDI approach for ovarian cancer, even if proteomics of this pathology are mainly explored (Longuespee et al., 2012b). A crosstalk between lipidomics and proteomics can enhance new concept describing the ongoing challenge of personalized therapies such as ''PI3Kness'' is doing with ovarian carcinoma (Bast and Mills, 2012). In a very near future, DALDI may find very relevant applications for a panel of pathologies implying lipids disorders such as Gaucher disease, coronary diseases, and Fabry disease, and many neoplastic afflictions such as liposarcomas or liver cancers. In these contexts, the identification of the detected lipids may be extremely relevant to characterize new molecular actors of the development of the pathologies. In this context, DALDI MSI approach can represents a direct translational link between classical and molecular histology.

Acknowledgments

We warmly thank the Ministère de L'Education Nationale, de L'Enseignement Supérieur et de la Recherche, Agence Nationale de la Recherche (ANR PCV to IF), région Nord-Pas de Calais (KA, RL) for financial supports. We are also thankful to Dr. David Buob from Laboratoire d'Anatomie et de Cytologie Pathologiques, Pôle Biologie Parc EURASANTE, CHRU Lille for the fruitful discussions related to lipid investigations in the field of anatomopathology.

Author Disclosure Statement

The authors declare that there are no conflicting financial interests.

References

Astigarraga E, Barreda-Gomez G, Lombardero L, et al. (2008). Profiling and imaging of lipids on brain and liver tissue by matrix-assisted laser desorption/ionization mass spectrometry using 2-mercaptobenzothiazole as a matrix. Anal Chem 80, 9105–9114.

Bast RC, Jr., and Mills GB. (2012). Dissecting ''PI3Kness'': The complexity of personalized therapy for ovarian cancer. Cancer Discov 2, 16–18.

Benabdellah F, Seyer A, Quinton L, Touboul D, Brunelle A, and Laprevote O. (2010). Mass spectrometry imaging of rat brain sections: Nanomolar sensitivity with MALDI versus nanometer resolution by TOF-SIMS. Anal Bioanal Chem 396, 151–162.

Bligh EG, and Dyer WJ. (1959). A rapid method of total lipid extraction and purification. Can J Biochem Physiol 37, 911–917.

Bonnel D, Longuespee R, Franck J, et al. (2011). Multivariate analyses for biomarkers hunting and validation through on-tissue bottom-up or in-source decay in MALDI-MSI: Application to prostate cancer. Anal Bioanal Chem 401, 149–165.

Burnum KE, Cornett DS, Puolitaival SM, et al. (2009). Spatial and temporal alterations of phospholipids determined by mass spectrometry during mouse embryo implantation. J Lipid Res 50, 2290–2298.

Calligaris D, Longuespee R, Debois D, et al. (2013). Selected protein monitoring in histological sections by targeted MALDI-FTICR in-source decay imaging. Anal Chem 85, 2117–2126.

Calvert GD, Blight L, Illman RJ, Topping DL, and Potter JD. (1981). A trial of the effects of soya-bean flour and soya-bean saponins on plasma lipids, faecal bile acids and neutral sterols in hypercholesterolaemic men. Br J Nutr 45, 277–281.

Caprioli RM. (2005). Deciphering protein molecular signatures in cancer tissues to aid in diagnosis, prognosis, and therapy. Cancer Res 65, 10642–10645.

Caprioli RM, Farmer TB, and Gile J. (1997). Molecular imaging of biological samples: Localization of peptides and proteins using MALDI-TOF MS. Anal Chem 69, 4751–4760.

Carden CP, Stewart A, Thavasu P, et al. (2012). The association of PI3 kinase signaling and chemoresistance in advanced ovarian cancer. Mol Cancer Therapeut 11, 1609–1617.

Carter CL, Mcleod CW, and Bunch J. (2011). Imaging of phospholipids in formalin fixed rat brain sections by matrix assisted laser desorption/ionization mass spectrometry. J Am Soc Mass Spectrom 22, 1991–1998.

Clark AE. (1947). A method for staining grossly fatty tissues with Scharlach R. J Pathol Bacteriol 59, 337.

Collin R, Griffith WP, Phillips FL, and Skapski AC. (1973). Staining and fixation of unsaturated membrane lipids by osmium tetroxide: Crystal structure of a model osmium(VI) intermediate. Biochim Biophys Acta 320, 745–747.

Collin R, Griffith WP, Phillips FL, and Skapski AC. (1974). Staining and fixation of unsaturated membrane lipids by osmium tetroxide. Crystal structure of a model osmium(VI) diester. Biochim Biophys Acta 354, 152–154.

Colsch B, and Woods AS. (2010). Localization and imaging of sialylated glycosphingolipids in brain tissue sections by MALDI mass spectrometry. Glycobiology 20, 661–667.

Dyatlovitskaya EV, Andreasyan GO, Malykh Ya N, Rylova SN, and Somova OG. (1997). Ganglioside shedding and changes in ceramide biosynthesis in human ovarian tumors. Biochemistry (Mosc) 62, 557–561.

El Ayed M, Bonnel D, Longuespee R, et al. (2010). MALDI imaging mass spectrometry in ovarian cancer for tracking, identifying, and validating biomarkers. Med Sci Monit 16, BR233–245.

Fournier I, Day R, and Salzet M. (2003). Direct analysis of neuropeptides by in situ MALDI-TOF mass spectrometry in the rat brain. Neuro Endocrinol Lett 24, 9–14.

Francese S, Bradshaw R, Flinders B, et al. (2013). Curcumin: A multipurpose matrix for MALDI mass spectrometry imaging applications. Anal Chem 85, 5240–5248.

Franck J, Arafah K, Barnes A, Wisztorski M, Salzet M, and Fournier I. (2009a). Improving tissue preparation for matrix-assisted laser desorption ionization mass spectrometry imaging. Part 1: Using microspotting. Anal Chem 81, 8193–8202.

Franck J, Arafah K, Elayed M, et al. (2009b). MALDI imaging mass spectrometry: state of the art technology in clinical proteomics. Mol Cell Proteomics 8, 2023–2033.

Franck J, Longuespee R, Wisztorski M, et al. (2010). MALDI mass spectrometry imaging of proteins exceeding 30,000 daltons. Med Sci Monit 16, BR293–299.

Fujiwaki T, Tasaka M, and Yamaguchi S. (2008). Quantitative evaluation of sphingomyelin and glucosylceramide using matrix-assisted laser desorption ionization time-of-flight mass spectrometry with sphingosylphosphorylcholine as an internal standard. Practical application to tissues from patients with Niemann-Pick disease types A and C, and Gaucher disease. J Chromatog B Anal Technol Biomed Life Sci 870, 170–176.

Fujiwaki T, Yamaguchi S, Tasaka M, Sakura N, and Taketomi T. (2002). Application of delayed extraction-matrix-assisted laser desorption ionization time-of-flight mass spectrometry for analysis of sphingolipids in pericardial fluid, peritoneal fluid and serum from Gaucher disease patients. J Chromatog B Anal Technol Biomed Life Sci 776, 115–123.

Fujiwaki T, Yamaguchi S, Tasaka M, Takayanagi M, Isobe M, and Taketomi T. (2004). Evaluation of sphingolipids in vitreous bodies from a patient with Gaucher disease, using delayed extraction matrix-assisted laser desorption ionization time-of-flight mass spectrometry. J Chromatog B Anal Technol Biomed Life Sci 806, 47–51.

Garrett TJ, and Dawson WW. (2009). Lipid geographical analysis of the primate macula by imaging mass spectrometry. Methods Mol Biol 579, 247–260.

Guenin E, Lecouvey M, and Hardouin J. (2009). Could a nano-assisted laser desorption/ionization target improve the study of small organic molecules by laser desorption/ionization time-of-flight mass spectrometry? Rapid Commun Mass Spectrom 23, 1395–1400.

Hayasaka T, Goto-Inoue N, Zaima N, Kimura Y, and Setou M, (2009). Organ-specific distributions of lysophosphatidylcholine and triacylglycerol in mouse embryo. Lipids 44, 837–848.

Ishida Y, Kitagawa K, Nakayama A, and Ohtani H. (2005). On-probe sample pretreatment for direct analysis of lipids in gram-positive bacterial cells by matrix-assisted laser desorption ionization mass spectrometry. Appl Environ Microbiol 71, 7539–7541.

Ishida Y, Madonna AJ, Rees JC, Meetani MA, and Voorhees KJ. (2002). Rapid analysis of intact phospholipids from whole bacterial cells by matrix-assisted laser desorption/ionization mass spectrometry combined with on-probe sample pretreatment. Rapid Commun Mass Spectrom 16, 1877–1882.

Ishida Y, Nakanishi O, Hirao S, et al. (2003). Direct analysis of lipids in single zooplankter individuals by matrix-assisted laser desorption/ionization mass spectrometry. Anal Chem 75, 4514–4518.

Jimenez CR, Li KW, Dreisewerd K, et al. (1998). Direct mass spectrometric peptide profiling and sequencing of single neurons reveals differential peptide patterns in a small neuronal network. Biochemistry 37, 2070–2076.

Kotelnikov VM, and Litinskaya LL, (1981). Comparative studies of Feulgen hydrolysis for DNA. I. Influence of different fixatives and polyethylene glycols. Histochemistry 71, 145–153.

Landgraf RR, Conaway MCP, Garrett TJ, Stacpoole PW, and Yost RA. (2009). Imaging of lipids in spinal cord using intermediate pressure matrix-assisted laser desorption-linear ion trap/orbitrap MS. Anal Chem 81, 8488–8495.

Lebaron FN, and Folch J. (1959). The effect of pH and salt concentration on aqueous extraction of brain proteins and lipoproteins. J Neurochem 4, 1–8.

Lillie RDA L. (1943). Supersaturated solutions of fat stains in dilute isopropanol for demonstration of acute fatty degeneration not shown by Herxheimer's technique. Archs Path 36.

Litman RB, and Barrnett RJ. (1972). The mechanism of the fixation of tissue components by osmium tetroxide via hydrogen bonding. J Ultrastruct Res 38, 63–86.

Longuespee R, Boyon C, Castellier C, et al. (2012a). The C-terminal fragment of the immunoproteasome PA28S (Reg alpha) as an early diagnosis and tumor-relapse biomarker: evidence from mass spectrometry profiling. Histochem Cell Biol 138, 141–154.

Longuespee R, Boyon C, Desmons A, et al. (2013a). Spectro-immunohistochemistry: A novel form of MALDI mass spectrometry imaging coupled to immunohistochemistry for tracking antibodies. Omics 2, 132–141.

Longuespee R, Boyon C, Desmons A, et al. (2012b). Ovarian cancer molecular pathology. Cancer Metastasis Rev 31, 713–732.

Longuespee R, Gagnon H, Boyon C, et al. (2013b). Proteomic analyses of serous and endometrioid epithelial ovarian cancers—Cases studies—Molecular insights of a possible histological etiology of serous ovarian cancer. Proteomics Clin Appl 7, 337–354.

Maneta-Peyret L, Compere P, Moreau P, Goffinet G, and Cassagne C. (1999). Immunocytochemistry of lipids: Chemical fixatives have dramatic effects on the preservation of tissue lipids. Histochem J 31, 541–547.

Meriaux C, Arafah K, Tasiemski A, et al. (2011). Multiple changes in peptide and lipid expression associated with regeneration in the nervous system of the medicinal leech. PLoS One 6, e18359.

Meriaux C, Franck J, Wisztorski M, Salzet M, and Fournier I. (2010). Liquid ionic matrixes for MALDI mass spectrometry imaging of lipids. J Proteomics 73, 1204–1218.

Mikawa S, Suzuki M, Fujimoto C, and Sato K. (2009). Imaging of phosphatidylcholines in the adult rat brain using MALDI-TOF MS. Neurosci Lett 451, 45–49.

Murphy RC, Hankin JA, and Barkley RM. (2009). Imaging of lipid species by MALDI mass spectrometry. J Lipid Res 50 Suppl S317–322.

Purbach B, Hills BA, and Wroblewski BM. (2002). Surface-active phospholipid in total hip arthroplasty. Clin Orthop Relat Res 115–118.

Riemersma JC. (1968). Osmium tetroxide fixation of lipids for electron microscopy. A possible reaction mechanism. Biochim Biophys Acta 152, 718–727.

Rujoi M, Estrada R, and Yappert MC. (2004). In situ MALDI-TOF MS regional analysis of neutral phospholipids in lens tissue. Anal Chem 76, 1657–1663.

Rujoi M, Jin J, Borchman D, Tang D, and Yappert MC. (2003). Isolation and lipid characterization of cholesterol-enriched fractions in cortical and nuclear human lens fibers. Invest Ophthalmol Vis Sci 44, 1634–1642.

Rylova SN, Somova OG, and Dyatlovitskaya EV. (1998). Comparative investigation of sphingoid bases and fatty acids in ceramides and sphingomyelins from human ovarian malignant tumors and normal ovary. Biochemistry (Mosc) 63, 1057–1060.

Snel MF, and Fuller M. (2010). High-spatial resolution matrix-assisted laser desorption ionization imaging analysis of glucosylceramide in spleen sections from a mouse model of Gaucher disease. Anal Chem 82, 3664–3670.

Sparvero LJ, Amoscato AA, Dixon CE, et al. (2012). Mapping of phospholipids by MALDI imaging (MALDI-MSI): Realities and expectations. Chem Phys Lipids 165, 545–562.

Sugiura Y, Konishi Y, Zaima N, et al. (2009). Visualization of the cell-selective distribution of PUFA-containing phosphatidylcholines in mouse brain by imaging mass spectrometry. J Lipid Res 50, 1776–1788.

Sugiura Y, Shimma S, Konishi Y, Yamada MK, and Setou M. (2008). Imaging mass spectrometry technology and application on ganglioside study; Visualization of age-dependent accumulation of C20-ganglioside molecular species in the mouse hippocampus. PLoS One 3, e3232.

Taketomi T, Hara A, Uemura K, and Sugiyama E. (1996). Rapid method of preparation of lysoglycosphingolipids and their confirmation by delayed extraction matrix-assisted laser desorption ionization time-of-flight mass spectrometry. J Biochem 120, 573–579.

Touboul D, Halgand F, Brunelle A, et al. (2004). Tissue molecular ion imaging by gold cluster ion bombardment. Anal Chem 76, 1550–1559.

Van Remoortere A, Van Zeijl RJ, Van Den Oever N, et al. (2010). MALDI imaging and profiling MS of higher mass proteins from tissue. J Am Soc Mass Spectrom 21, 1922–1929.

Veloso A, Astigarraga E, Barreda-Gomez G, et al. (2011). Anatomical distribution of lipids in human brain cortex by imaging mass spectrometry. J Am Soc Mass Spectrom 22, 329–338.

Vidova V, Pol J, Volny M, et al. (2010). Visualizing spatial lipid distribution in porcine lens by MALDI imaging high-resolution mass spectrometry. J Lipid Res 51, 2295–2302.

Wang HY, Wu HW, Tsai PJ, and Liu CB. (2012). MALDI-mass spectrometry imaging of desalted rat brain sections reveals ischemia-mediated changes of lipids. Anal Bioanal Chem 404, 113–124.

Wang X, Han J, Pan J, and Borchers CH. (2014). Comprehensive imaging of porcine adrenal gland lipids by MALDI-FTMS using quercetin as a matrix. Anal Chem 86, 638–646.

Yappert MC, Rujoi M, Borchman D, Vorobyov I, and Estrada R. (2003). Glycero- versus sphingo-phospholipids: Correlations with human and non-human mammalian lens growth. Exp Eye Res 76, 725–734.

Address correspondence to:
Isabelle Fournier
Laboratoire PRISM
Bâtiment SN3 1^{e} étage
Avenue Paul Langevin 59650
Villeneuve D'Ascq
France

E-mail: isabelle.fournier@univ-lille1.fr

or

Michel Salzet
Laboratoire PRISM
Bâtiment SN3 1^{e} étage
Avenue Paul Langevin 59650
Villeneuve D'Ascq

E-mail: michel.salzet@univ-lille1.fr